15

X-ray crystal cavity and resonators

© V.V. Lider

Kurchatov Complex Crystallography and Photonics, NRC "Kurchatov Institute", 119333 Moscow, Russia e-mail: vallider@yandex.ru

Received January 22, 2025 Revised February 24, 2025 Accepted March 9, 2025

The review considers various configurations of crystal cavities for X-rays. X-ray resonators, including the Fabry-Perot resonator, are described. Particular attention is paid to the methods of coupling a crystal cavity with X-ray free-electron laser.

Keywords: X-rays, crystal cavity, backscattering, resonators, free-electron laser.

DOI: 10.61011/TP.2025.08.61725.7-25

Introduction

The crystal cavity is a device that can circulate X-rays along a closed trajectory as a result of subsequent reflections. These devices include, for example, X-ray resonators of various configurations [1–4]. As a result of multiple convolution of energy distribution of quanta, only quanta with energies that correspond to an exact condition of Bragg reflection "survive" thereby resulting in narrowing a spectrum transmittance bandwidth of the cavity. Thus, an essential feature of the resonators is their capability of forming an X-ray beam in a narrow spectrum interval, thereby creating great opportunities for ultra-monochromatization of X-rays.

Recently, a concept of an X-ray free-electron laser (FEL) with a feedback attracts attentions of researchers. The crystal cavity is used as the feedback [5]. An output signal of a FEL amplifier is stored and recirculated in the cavity so as an X-ray pulse could interact with subsequent fresh electron bunches during multiple passes between crystal reflectors, thereby increasing intensity of radiation inside the filter with each pass, filtering the spectrum and improving coherency of radiation at its output. Thus, symbiosis of the X-ray FEL with its unique characteristics and the crystal cavity provides great opportunities for carrying out high-accuracy time-resolution experiments [6].

The aim of the present review is to introduce the reader to a history of designing, using as well as capabilities of improvement of the crystal cavity for X-rays.

1. X-ray resonators

The X-ray resonators can be used for high-resolution spectroscopy and interferometry. In the hard X-ray range, the energy resolution $\sim \mu eV$ can be obtained using these devices. It will make it possible to study dynamics of biological macromolecules and phonon spectra in condensed medium with energy resolution that is much higher than

before. The crystal resonators can be cut out of a solid crystal ingot [2]. A geometry fixes not only a ratio between a diffraction angle and an energy photon, but an X-ray trajectory condition as well. However, for exact compliance of the radiation wavelength λ and the Bragg angle θ dictated by the diffraction condition $\lambda = 2d \sin \theta$, it is usually necessary to "adjust" a resonator's interplanar spacing by varying the monoblock temperature (Fig. 1, a, b).

However, the monoblock resonators practically exclude their tunability to another wavelength. It would be desirable to have an accurately tunable design that is not based on the random ratio of the wavelength and the Bragg angles. In the studies by Bond et al. [1], Cotterill et al. [3], these limitations were lifted by the noncomplanar geometry of diffraction in the former case and by a possibility of intersection of the XR trajectories inside the cavity in the latter. Fig. 1, c shows the pathway of the rays in the resonator with the same Bragg reflectors that are parallel in pairs. The number of the reflectors N is determined by a value of the Bragg angle θ from the condition $90^{\circ}/\theta < N/2 < 180^{\circ}/\theta$ [7]. The length of a resonance wave can be changed by varying mutual orientation of the crystals in the resonators.

One of the problems of the X-ray resonators is entry/exit of the X-rays into/out of the cavity. The study by Kolpakov et al. [8] proposes to solve the problem by introducing a single crystal with a thickness that ensures the Bormann effect into one of the resonator branches [9]. The problem can be solved by parallel shift of one of the reflectors along its diffraction vector, which results in disruption of the beam trajectory closedness while maintaining cyclicity inside the resonator [7]. With each complete cycle, the beam makes a parallel shift by the constant step *a*, whose value is determined by the geometry and a value of reflector rearrangement.

$$a = 2(b_{14} - b_{23})\cos\theta,\tag{1}$$

where b_{14} and b_{23} are distances between the reflectors M1, M4 and M2, M3, respectively; θ is the Bragg angle of

16 1361

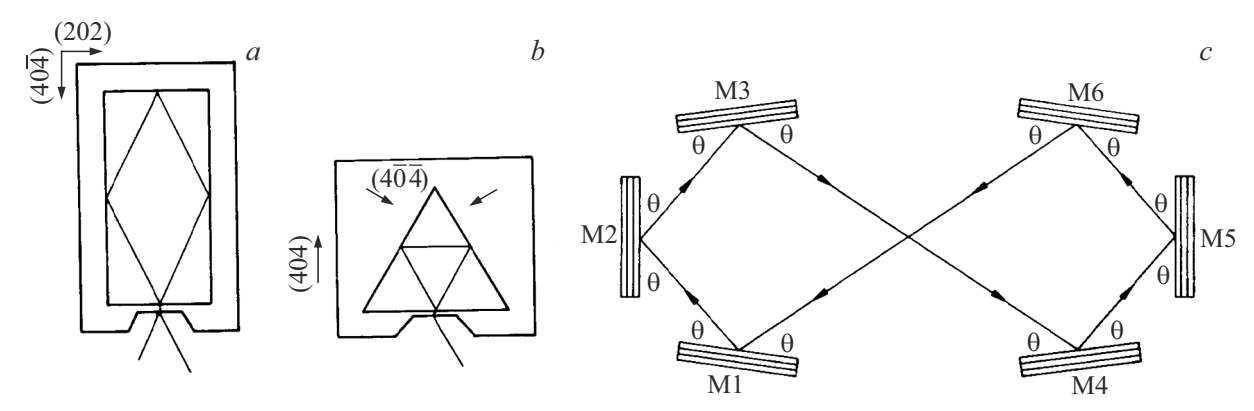


Figure 1. Diagrams of X-ray pathway in the crystal resonators. The rectangular germanium monoblock resonator (a) is tuned to the $CoK_{\alpha 1}$ line at the temperature of 35°C, whereas the triangular resonator (b) made of silicon will require deep cooling for tuning to the $NiK_{\alpha 2}$ line [2]. In the complanar resonator (c), the crystal reflectors M1 and M6 are parallel, so are M2 and M5, M3 and M4 [3].

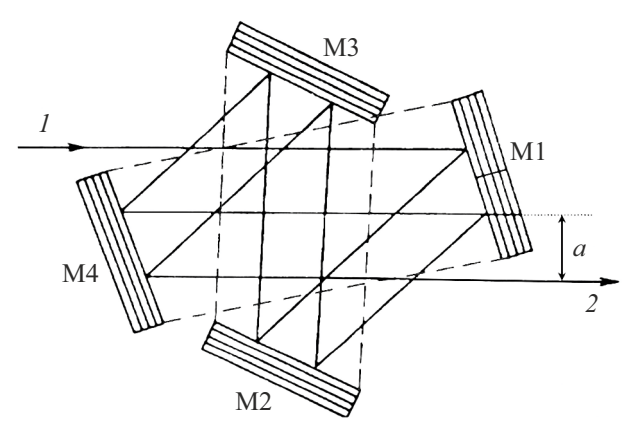


Figure 2. Diagram of input/output of X-rays in the two-cycle four-crystal resonator with mutually parallel reflecting planes for the crystals M1, M4 and M2, M3 (I — the primary XR beam, a — the shift of the beam 2 at the resonator output) [7] (see explanations in the text).

the resonance wave. This reflector rearrangement results in formation of a separate free input of the primary beam and an output of the monochromatized beam (Fig. 2).

Crystal cavity for backscattering of X-rays

Backscattering was reviewed for the first time from the point of view of a dynamic theory of X-ray diffraction on a perfect crystal by Kohra and Matsushita in 1972 [10]. Even this early paper already noted interesting features of backscattering: when the Bragg angle approaches 90° $(\theta \to \pi/2)$, a width of its rocking curve sharply increases, while an energy transmittance bandwidth of the crystal sharply decreases.

$$(\Delta E)_{\pi/2}/E \approx 1/\pi N_d,\tag{2}$$



Figure 3. Silicon crystal cavity when using backscattering (reflection (888)). The beams t_0 and t_1 at the cavity output correspond to a zero and a single cycle of X-ray reflection from its walls [12,13].

where N_d — the number of the reflecting planes that "fit" within the extinction length $\Lambda_{\pi/2}(\Lambda_{\pi/2} \approx \lambda/|\chi_{hr}|, \lambda$ —the XR wavelength, χ_{hr} —the real part of the Fourier component of crystal polarizability.

Thus, it was possible to create X-ray high-numerical-aperture optics that is based on backscattering and has high energy resolution. After that, there was a lot of publications dedicated to use of X-ray backscattering in X-ray high-resolution optics, metrology as well as for structural characterization of various crystal items [11].

The authors of the papers [12,13] have studied time distribution of radiation intensity at the output of the crystal cavity that is irradiated by a short pulse of synchrotron radiation. The monolith silicon cavity consisted of a pair of vertically-arranged wall-reflectors separated by the distance of 150 mm (Fig. 3). The walls were like a wedge designed to vary its effective thickness within the interval $50-500\,\mu\text{m}$. Backscattering was implemented by using the reflection (888) at the Bragg angle of 89.865° . At the same time, the energy of the X-ray beam was $15.817\,\text{keV}$, whereas the energy resolution was $3.7\,\text{meV}$.

The time response of the cavity to the pulse of duration of $100 \, \mathrm{ps}$ is shown on Fig. 4, a. The width of $500 \, \mathrm{ps}$ (the curve I) corresponds to the detector response to the primary pulse without the resonator when t=0. The time pattern with the resonator in a position of Bragg diffraction substantially differs from the first curve and is a series of exponentially damped oscillatory maximums with the period of $1.0 \, \mathrm{ns}$. The maximums correspond to quanta that

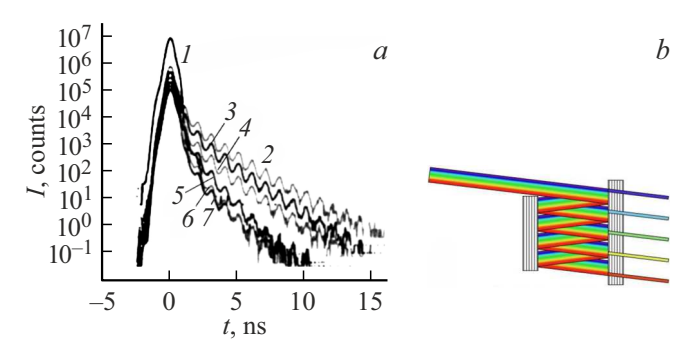


Figure 4. a — the time distribution of radiation intensity at the output of the crystal cavity after its irradiation by the pulse of duration of 100 ps in the backscattering mode: the wall thickness: the curve 2-243, 3-292, 4-342, 5-388, 6-425, $7-456\,\mu\mathrm{m}$; 1— the primary pulse [13]; b— a diagram of the open-contour delay line. Holes in one of the crystal select different parts of the cross section of the initial beam with different time delays [13].

are "arrested" by the cavity with 1, 2, 3,... n subsequent reflections from both walls. As the walls for X-rays are translucent, then after each "double" act of backscattering a small portion of the quanta "leaks" through the output wall of the cavity.

The X-ray free-electron lasers can require various types of the delay lines and storage devices. The subsequent photon bunches can be separated, for example, by using the crystal cavity that is provided in the studies of Liss et al. [12,13]. Besides, this optics is not limited by closed-contour devices and can overcome the input-output problem by creating several holes in one of the reflectors (Fig. 4, b).

The studies [12,13] have reviewed a noncoherent method of storage of X-ray photons in the cavity. Additional coherent interference that takes place in the Fabry-Perot resonator will result in sharp reduction of the spectrum transmittance bandwidth of the cavity.

3. X-ray Fabry-Perot resonators

The Fabry-Perot resonators are standard instruments in the visible light optics. They were invented by Fabry and Perot [14] and have been used as narrow-band filters for more than one hundred years as instruments for measuring the spectrum line width and the wavelength. The main components of the simplest Fabry-Perot resonator are two high-quality flat mirrors with a fixed distance between them.

An idea of the X-ray Fabry-Perot resonator (XFPR) was suggested by Steyerl and Steinhauser [15] in 1979 and consisted in replacing optical mirrors with crystal mirrors. They also considered a problem of spurious (multiwave) reflections that occur in silicon crystals with accurate normal incidence to reflecting atomic planes [16] and warned that these spurious reflections will sharply reduce reflectivity of the mirror and worsen efficiency of the proposed device. Based on the dynamic theory of

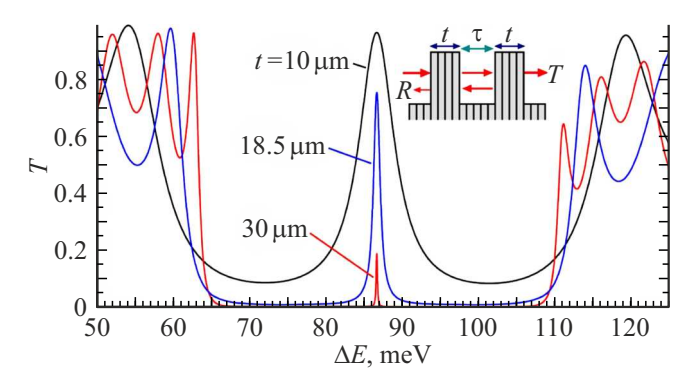


Figure 5. Transmittance spectra of the diamond XFPR (the reflection (224)) for various thicknesses of the crystal plates t, $\tau = 10.9 \,\mu\text{m}$. The incident angle is $90^{\circ} - 0.5 \,\text{mrad}$ for excluding multiwave diffraction [23].

diffraction, the studies [17–19] have developed a theory of X-ray Fabry-Perot interferometer. The XFPR theory was further developed in the paper [20] by taking into account possible imperfections (roughness of working surfaces, nonparallelism and inhomogeneity of the mirror thicknesses, the temperature gradient). The XFPR theory is quite fully described in the studies of Shvyd'ko [21,22].

The external X-ray radiation penetrates the resonator cavity through the first crystal mirror and circulates inside the resonator, reflecting from the crystal mirrors (see the insert of Fig. 5). The system becomes transparent despite good reflectivity of the crystal mirrors, when the distance between the mirrors is equal to an even number of radiation wave half-periods: in this case a resonance condition of formation of a standing X-ray wave in the cavity is fulfilled. The geometry of back scattering is important for minimizing effect of finite divergence of the beam on resolution of the Fabry-Perot resonators.

The energy distance E_f between the adjacent resonances is called a free spectrum interval and is a constant value that does not depend on the energy of the primary beam:

$$E_f = \hbar c / 2L_\tau. \tag{3}$$

Here \hbar — the Planck constant, c — the speed of light, L_{τ} — the effective distance between the mirrors. The spectrum width of transmittance resonances Γ is smaller the higher reflectivity R of each mirror: $\Gamma = E_f(1-R)/\pi R^{1/2}$.

Resolution of the cavity is determined as a ratio of the distance between the resonances and the resonance's spectrum width Γ :

$$F = E_f/\Gamma = \pi(R)^{1/2}/(1-R). \tag{4}$$

Therefore, the spectrum width of transmittance resonances Γ is smaller the higher reflectivity of each mirror R.

It is shown in the papers [21,22] that the resolution discloses an effective number N_s of multiple backscattering acts that participate in formation of the standing wave: $F = 2N_s$.

Owing to multiple diffraction, the XFPR is a device with $F \gg 1$: for the mirror with the value R = 0.85, F = 19.3, while for R = 0.9, F = 29.8.

High resolution of the cavity also determines a very narrow energy transmittance bandwidth $(\Delta E/E)_p$ of the XFPR:

$$(\Delta E/E)_p = (FN_\tau)^{-1},\tag{5}$$

where N_{τ} is the number of reflecting planes that fit within the effective distances between the mirrors L_{τ} . Since during Bragg diffraction the X-rays penetrate into the crystal for the extinction depth $\Lambda_{\pi/2}$, the effective distance between the mirrors $t > \Lambda_{\pi/2}$ will be determined by the formula $L_{\tau} = \tau + 2\Lambda_{\pi/2}$ [18].

Thus, in terms of energy resolution the XFPR significantly exceeds the single Bragg reflection: first of all, $N_{\tau} \gg N_d$ (see the formula (2)), as it is possible to manufacture the cavity with a gap between the mirrors, which significantly exceeds the extinction length of the crystal; secondly, due to multiple diffraction inside the cavity $F \gg 1$.

High, almost theoretical reflectivity of sapphire during backscattering from the atomic planes $(0\ 0\ 0\ 30)$ was experimentally demonstrated in the first X-ray Fabry-Perot interferometer [24]. In 2005, the experiment has produced the XFPR using synchrotron radiation and two silicon crystal plates with the reflection (12 4 0), of the thickness $25-150\,\mu\mathrm{m}$ and the gap $40-150\,\mu\mathrm{m}$ with energy resolution $\Delta E = 0.36 \,\mathrm{meV}$ when $E = 14.4388 \,\mathrm{keV}$ [25]. In order to increase efficiency of the resonator, the study of Tsai et al. [26] used sapphire plates. In comparison with the silicon resonator, the sapphire XFPRs not only have a lower absorption coefficient, but they also can avoid effects of multiwave diffraction that reduces backscattering intensity due to redistribution of the energy of the primary beam between excited sites of a reciprocal lattice. The thickness of the crystal plates and the gap between them were designed to be 40 and 90 mm, respectively, while the reflection (0 0 0 30) was used for backscattering at 14.3147 keV.

One of the methods of increasing the resonator resolution is to correctly choose a thickness of the crystal reflectors. Fig. 5 shows a capability of making a sharper resonance by increasing the thickness of the reflectors. Transmission curves were calculated by authors of the paper [23] for the flat primary wave. The single cavity has maximum efficiency of the resonance only when the two plates have the same thickness t. When $t = 10 \,\mu\text{m}$ T = 96 % (Fig. 5). However, the full width at half maximum (FWHM) of a resonance peak is $\delta E = 5.8$ meV, which corresponds to a low F = 5.2. Meanwhile, the background in addition to the resonance peak is high (> 8%). It is obvious that it is related to low reflectivity R = 59% of the plates with $t = 10 \mu m$. R can be improved by increasing t. When $t = 18.5 \,\mu\text{m}$, R is 90 %, whereas the width of the resonance peak δE becomes equal to 1 meV in Fig. 5 when F = 30. But the peak still has extended "tails" and the background is still noticeable. Moreover, clarity improvement is accompanied by drop of the peak efficiency to T = 75% (for example, for silicon

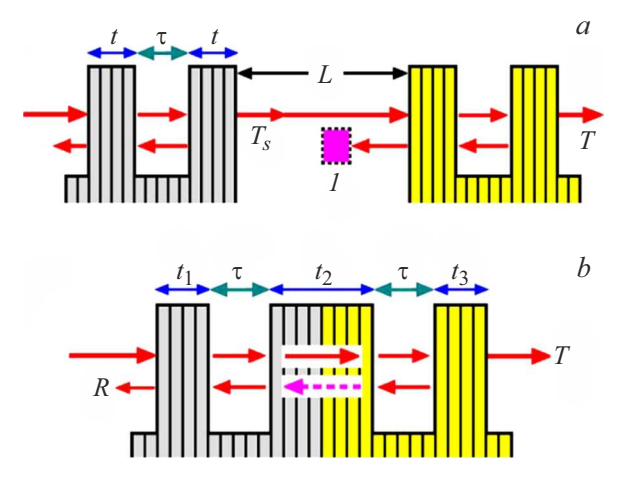


Figure 6. a — successive (cascade) single-cavity resonators (I — the insulator); b — the monolith two-cavity resonator [23].

crystals with higher absorption the efficiency drops more sharply with increase of t). For $t = 30 \,\mu\text{m}$ ($R_c = 98 \,\%$) T is just 18 %, although the peak becomes extremely narrow: $\delta E = 0.19 \,\text{meV}$. Therefore, usually one resonator can not simultaneously provide high energy resolution and good efficiency, especially for high-absorption crystals. This disbalance can be overcome by successive cascading of two single-cavity resonators, as shown in Fig. 6, a.

However, here a reverse wave from the second resonator can either form undesirable resonance in a gap between the two resonators or enter the first cavity and attenuate the resonance. Therefore, the "insulator" that absorbs this wave is desirable. In this condition, the transmission ratio is just $T = T_s^2$, where T_s is transmittivity of one resonator.

In comparison with the transmission curve of the single resonator with $t=10\,\mu\mathrm{m}$ in Fig. 5, b, here the peak is narrower, $\delta E=3.75\,\mathrm{meV}$, while the peak efficiency is still higher, $T=92\,\%$. What is even more important, is that the background is noticeably suppressed, although R is just $59\,\%$.

Since cascading of the two resonators requires rigorous adjustment, stability and control of the temperature, the much simpler diagram is to combine two middle plates in Fig. 6, a so that the two resonators become a monolith two-cavity resonator (Fig. 6, b).

Usually, for the *N*-cavity resonator (N > 1) with the plates of the same thickness, the resonance peak is divided into *N* sub-peaks. Thus, for correct operation of the multicavity resonator, the thickness of the plates shall be correctly selected. When $t_2 < 2t_1$, the peak is always divided, but the two sub-peaks tend to merge only when $t_2 \to 2t_1$. When $t_2 = 2t_1$, the sub-peaks become a single peak. With further increase of t_2 , the peak is no longer divided. Instead, the width of the peak is reduced, but the peak efficiency is reduced as well (the curve with $t_2 = 30 \,\mu\text{m}$). So, $t_1 = t_3 = t_2/2$ is an optimal condition (which is always true for any Bragg reflections). For example, in Fig. 7, *b* when $t_1 = t_3 = 20 \,\mu\text{m}$, the optimal value of t_2 is also doubled to

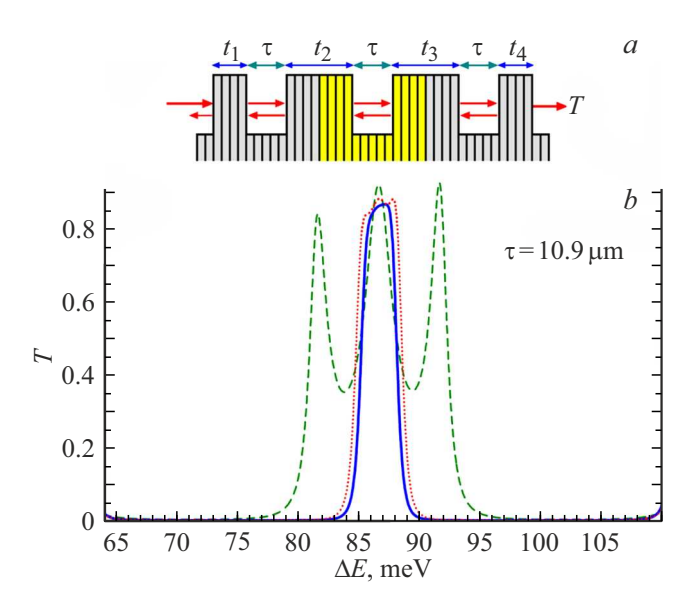


Figure 7. a — the diagram of the three-cavity resonator; b — the transmission curves of the three-cavity diamond resonator (reflection (224)). $t_1 = t_4 = 10 \,\mu\text{m}$. The dashed line: $t_2 = t_3 = 10 \,\mu\text{m}$. The dotted line: $t_2 = t_3 = 20 \,\mu\text{m}$. The solid line: $t_2 = t_3 = 22 \,\mu\text{m}$ [23].

 $40 \,\mu\text{m}$. Note that here the peak efficiency is $52 \,\%$, whereas the width of the peak is just $0.45 \,\text{meV}$ (F = 67).

Combinations (t_1, t_2, t_3) that do not satisfy the condition $t_1 = t_3 = t_2/2$, result either in splitting of the peaks or in reduction of the efficiency. The optimal condition $t_1 = t_3 = t_2/2$ indicates that the two-cavity resonance mechanism is really similar to the mechanism of the two cascade single-cavity resonators.

Let us note that the reverse wave (the dashed line in Fig. 6, b) is always weak for $t_1 = t_3 = t_2/2$. the two cavities to large extent are independent of each other, except that the first cavity ensures a one-side inlet into the second cavity, i.e. the resonance processes of the two cavities in Fig. 7, b occur sequentially with slight interaction. The considered mechanism can be also applied to the N-cavity resonators (N > 2). For example, when the three-cavity resonator consists of the plates of the same thickness (Fig. 7, a), the resonance peak is divided into three sub-peaks (Fig. 7, b). The sub-peaks merge when t_2 and t_3 are doubled. Thus, the three-cavity resonator is (almost) equivalent to the three cascade single-cavity resonators. Here, the resonator with $t_2 = t_3 = 2t_1 = 2t_4$ has small bulges on the resonance peak, which, however, can be eliminated by slightly increasing t_2 and t_3 above $2t_1$, as on the curve with $t_2 = t_3 = 22 \,\mu\text{m}$ in Fig. 7, b.

One of the main special features of the XFPR is a narrow transmittance bandwidth that transforms it into an energy filter with high selectivity. This feature makes it possible to use the XFPR for high-resolution spectroscopy. Fig. 8, a shows a possible experimental diagram for measuring the spectra of nuclear resonance scattering (NRS) of X-rays [21,27].

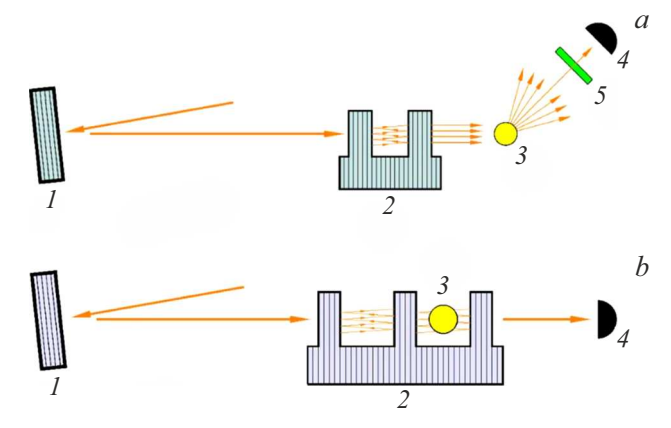


Figure 8. Experimental diagrams using the XFPR: a — for measuring the spectra of inelastic nuclear resonance scattering of X-rays [20]; b — for obtaining a phase-contrast images of the studied sample [21] (I — the backscattering high-resolution monochromator, 2 — XFPR, 3 — the sample, 4 — the detector, 5 — the analyzer of X-ray nuclear resonance scattering).

For example, the reflection α -Al₂O₃(1 6 -7 22) of the high-resolution monochromator with energy resolution of 1.9 meV, when $T=150\,\mathrm{K}$, corresponds to the energy of 14.4125 keV of nuclear resonance of the $^{57}\mathrm{Fe}$ sample. For this energy, the best choice is the reflection α -Al₂O₃ (1 3 -4 28) of the XFPR. When $\tau=280\,\mu\mathrm{m}$ and $t=150\,\mu\mathrm{m}$, the energy resolution of the optical system is $\Delta E/E\approx 10^{-8}$. But even though, in terms of energy resolution the XFPR probably will not be advantageous over recent designs of the single-crystal monochromators [28], it shall exceed them by a quite large value of the receiving angle $\sim 10^{-4}\,\mathrm{rad}$ [21].

The monochromatized beam at the FXPR output also has ultrahigh time coherency due to the narrow spectrum transmittance bandwidth. Its high phase sensitivity that increases with increase of Q factor of the crystal cavity can ensure an advantage of the XFPR over the common methods for obtaining phase contrast [29].

Since obtaining phase contrast by means of the XFPR requires that the spectrum width of the primary beam be less than the width of resonance [21], a "composite" XFPR with the two identical cavities should be used (Fig. 8, b). At this, the first cavity serves as an energy filter that forms the beam with pre-defined parameters, while the second one functions as an interferometer. Placing the studied item into it results in resonance shift and subsequent change of intensity of the transmitted beam [21].

4. Crystal cavity for the X-ray free-electron laser

In two recent decades, successful operation of X-ray single-pass free-electron lasers with extreme brightness, transverse coherency and an ultra-short pulse length [30] has paved the way for diverse scientific applications in the fields of physics, biology, chemistry and medicine due to

its advantages: a short wavelength, high energy and good coherency [31,32].

However, these pulses of the X-ray free-electron pulses, which are mainly based on selfamplified spontaneous emission (SASE) that occurs due incoherent shot noise, usually have poor longitudinal coherency. Along with various diagrams of self-nucleation for improvement of longitudinal coherency of SASE XFEL pulses [33,34], the cavity-based x-ray free-electron laser (CBXFEL) like an x-ray free-electron laser oscillator (XFELO) [5,35,36] or an x-ray regenerative free-electron laser amplifier with a high amplification coefficient (XRAFEL) [37-39] is a promising candidate for obtaining high-brightness X-rays with full (transverse and longitudinal) coherency and good stability. The XFELO and XRAFEL concepts are based on the same fundamental ingredients to implements their full capabilities. Each diagram requires an electron beam with high repetition rate, an undulator for ensuring FEL amplification and an X-ray crystal resonator for recirculation and monochromatization of X-ray radiation. The main difference between the two modes is a peak current of electrons and a bunch length [40].

CBXFEL uses the X-ray cavity for monochromatization and storage of a portion of the recirculating X-ray pulse so that it can interact with subsequent fresh electron bunches during multiple passes. It is expected that the CBXFEL pulse will have full coherency and the narrow energy transmittance bandwidth, which can be just several meV for XFELO [35,36,41].

Power variation in CBXFEL can be described as follows [40]:

$$P_n = R(1+G)P_{n-1}, (6)$$

where P_n — the power of the X-ray pulse with the n-th pass through the resonator, G — the FEL amplification coefficient, while R — full reflectivity of the optical resonator. The amplification coefficient per one pass is R(1+G), and the power increases if R(1+G) > 1. When R(1+G) = 1, the system gets to its stable state.

The simplest cavity is formed by two crystal mirrors with normal incidence [35,42]. In this case the reflectors shall be a sapphire crystal (Fig. 9, a) in order to avoid effects of multiwave diffraction of Si and C crystals of the cubic crystal system, which result in low reflectivity that is related to the condition of exact backscattering [22,24].

The crystal cavity shall also ensure focusing for controlling an inter-resonator mode profile. A promising option is to use parabolic compound refractive lenses (CRL) [43] (Fig. 9, a). An grazing-incidence ellipsoid mirror can be used for focusing as well as for closing the contour, when the crystal reflectors are not in exact backscattering (Fig. 9, b). In this case it is preferable to use single-crystal diamond. It was demonstrated that the mirrors made of diamond crystals achieve almost 100% of reflectivity [44]. Due to unique combination of excellent properties including high thermal conductivity, high mechanical and radiation

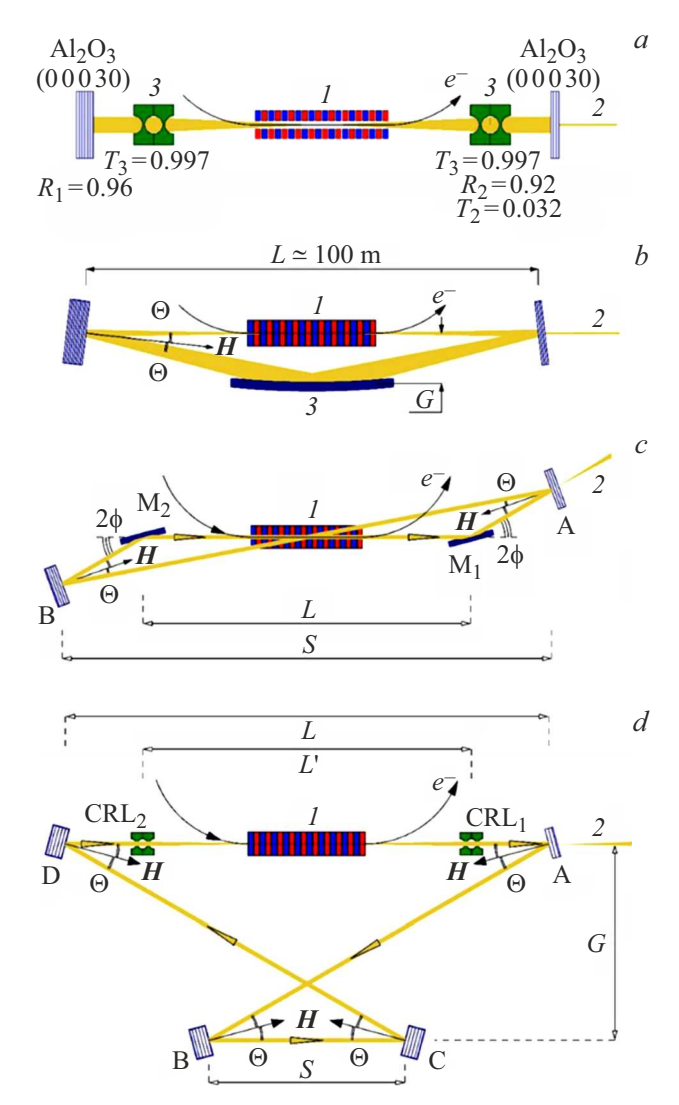


Figure 9. Diagrams of the X-ray resonator with two (a-c) and four (d) crystals: I — the undulator, 2 — the X-ray beam at the cavity output, 3 — the focusing optical elements [35,36] (see explanations in the text).

strength, the diamond crystals are a perfect choice for the crystal mirrors in CBXFEL.

A structure of the cavity made up of the two mirrors is simple but it has two basic shortcomings [36]. First of all, not all the types of the crystals can be used as reflectors due to the effect of multiwave diffraction. Secondly, the operating energy of these cavities is not restructured, because the Bragg angle can not be changed. A configuration of the resonator that consists of the two crystals with almost normal incidence and the grazing-incidence mirror, which is schematically shown in Fig. 9, b, is a candidate for the tunable resonator. Here, the crystals are oriented so that the incident and outgoing X-rays in each crystal form the same incident angle Θ in relation to the diffraction vector H that is normal to reflecting atom planes ($\Theta = \pi/2 - \theta$, θ is the Bragg angle).

The photon energy E can be varied by changing the distance G and reorienting the crystals to maintain Bragg reflection. However, a tuning range in this configuration is limited by the requirement that the grazing incident angle 2Θ to the mirror is less than the critical angle $\theta_{\rm cr}$ of full external reflection. For the photon energy $E\approx 10\,{\rm keV}$, usually $\theta_{\rm cr}\approx 1\,{\rm mrad}$. This requirement makes it possible to retune the X-ray energy within a very small range.

Fig. 9 shows a similar configuration with the two mirrors M_1 and M_2 . This configuration can be more favorable for controlling the mode profile and optimizing a relation of the X-ray and electron beams, but it also has a very limited tuning range because of the small grazing angle $\phi \approx 1$ mrad.

However, the resonator that uses the four crystals and intersecting X-ray trajectories can be tunable according to the diagram (Fig. 1, c) that was first proposed by Cotterill in 1968 [3].

In Fig. 9, d, the crystals A, B, C and D are arranged in four angles of an isosceles trapezoid and the X-rays propagate along a zig-zag trajectory. The length L of the path AD is great, about 100 m for the examples that are considered in the paper [35]. It would be convenient to fix the positions A and D so that the length L was constant. It would be useful to select the length S of the path BC to be short (several meters or less) so that the crystals B and C could be arranged on one optical table. The crystal shall be oriented so that the Bragg condition is satisfied for each crystal. Then, the incident angle is the same for all the crystals and related to trapezoid sizes by the relationship

$$tg 2\Theta = 2G/(L+S), \tag{7}$$

where G is a distance between two parallel paths AD and BC

The length of the X-ray path in one cycle is determined as

$$l = (L+S)(1+\cos 2\Theta)/\cos 2\Theta. \tag{8}$$

It is necessary that l would not vary when tuning the cavity, as the time of circular pass should be constant with high accuracy and equal to a time interval between two adjacent electron bunches. The energy of the X-ray photon is tuned by changing Θ , which in turn requires changing G and S. A critical point here is that the lines AD and BC are parallel, so the angle Θ is the same in all the four positions of the crystal. By combining the equations (7) and (8), we obtain

$$G = (l/2) \operatorname{tg} \Theta, \tag{9}$$

$$L + S = (l/2)(1 - tg^2 \Theta).$$
 (10)

The equations (9) and (10) determine a way of how G and S shall vary when changing the angle Θ during tuning the cavity, wherein I and L are supposed to be fixed parameters. In order to increase the photon energy E, the incident angle Θ must be increased. Then the distance G shall be increased in accordance with the equation (9). Similarly, the distance S must be reduced in accordance

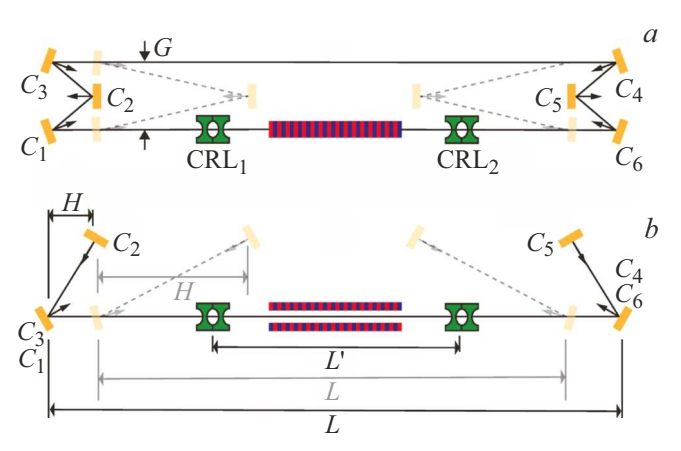


Figure 10. Schematic view of the 6-mirror ring resonator for the X-ray FEL oscillator using the flat Bragg mirrors $C_1 \ldots C_6$ and the compound refractive lenses CRL_1 and CRL_2 for focusing (a - top view, b - side view) [45].

with the equation (10) [36]. Here, the Bragg angle can be changed within the range $45^{\circ} < \theta < 90^{\circ}$.

The papers [38,45] consider a tunable six-crystal compact cavity (Fig. 10). The crystals are arranged in a non-complanar geometry of scattering. There are two units that comprise three crystals (C_1 , C_2 and C_3) on one side of the undulator and three crystals (C_4 , C_5 and C_6) on the other side. Collimating and focusing elements are shown as $CRL_{1,2}$ which could have been glazing incidence mirrors, but they are shown in the figure in another possible alternative - compound refractive lenses. By presuming that all the crystals and reflections of Bragg are the same, the Bragg angles can be selected within a wide range $30^{\circ} < \theta < 90^{\circ}$.

The resonator allows tuning the photon energy in a large spectral range by synchronously varying all the Bragg angles. Besides, in order to ensure a constant time of flight, the distance L (which limits the undulator) and the distance between the crystals, which is characterized by H, must vary together with θ . When tuning the resonator, the side size G remains constant. Since the lines C_1C_6 and C_3C_4 are fixed, inter-resonator radiation can be simultaneously output for several users in different locations of the resonator. Output through the crystals C_1 and C_4 is the most favorable, as a direction of output beams does not change with the photon energy, but it is also possible to output through the crystals C_3 and C_6 for more users.

Unlike typical table resonators of the optical lasers, CBXFELs will require a much larger size, often approaching hundreds of meters in length. This is due to physics of an amplifying medium and a process of amplification of the X-ray free-electron lasers. Amplification requires interaction between the X-ray pulses with a sequence of the relativistic electron bunches through long undulators. The repetition rate of an electron source, which determines the time of transmission through the cavity, is adjusted by available accelerators of high-brightness electrons. For the modern

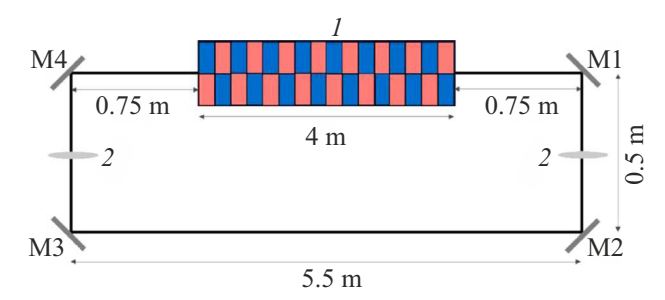


Figure 11. Design of the 12-m crystal cavity (I — the undulator, 2 — the optical focusing elements) [47].

superconducting linear accelerator with the repetition rate in a scale of MHz, it specifies a resonator length of about 100 m. The large sizes of the resonators, in turn, require very strict spatial and angular tolerances and requirements to a system of the Bragg mirrors [46].

When trying to reduce the CBXFEL size, researchers proposed various innovative methods of "miniaturization" of these devices.

For example, the studies [46,47] have used the most compact rectangular cavity with four diamond crystals and a circular bypass length 14.2 [46] and 12 m [47] (Fig. 11).

In order to increase inter-resonator power, the study [47] has used from six to eight electron pulses that were generated by an ultra-compact X-ray free-electron laser (UC-XFEL) [48] with a periodicity of 40 ns. The resonance energy was centered at 6.95 keV (reflection (220), $\theta = 45^{\circ}$). The thickness of the first-mirror crystal M1 was $20\,\mu\text{m}$, which provided reflectivity of 98.9 %. The mirrors M2–M4 had a thickness of $100\,\mu\text{m}$ with reflectivity of 99.6 %.

As in the case of the X-ray resonators, the method of outputting radiation out of the cavity is one of the most important components for CBXFEL. Reduction of the thickness of the crystal mirror is one of the ways of outputting X-ray radiation [35]. However, it is difficult to manufacture a thin crystal without introducing defects; moreover, it is almost impossible to fasten it without stresses by a mechanically stable method. The crystals of a drum head, which are monolith crystal structures that consist of a thin membrane fitted with a surrounding thick solid collar, are a solution that provides a mechanically stable and stressfree fastening of the thin membrane with effective heat transfer [41,49].

A standard approach of using the thin-crystal reflecting mirrors is very often limited by extracting only several percent of intensity of the beam that is formed inside the cavity (Fig. 9, a). It is acceptable for the x-ray free-electron laser oscillators with a low amplification coefficient. However, the regenerative free-electron laser amplifier with the high amplification coefficient requires much higher efficiency of outputting. Another solution of the problem is to use the Bragg mirror with a pinhole for transmission of a portion of intensity formed in the cavity [38,39].

An alternative method of extracting the inter-cavity X-ray pulse both for the cavity-based FEL with the high amplification coefficient and the cavity-based FEL with the low amplification coefficient is to use inter-cavity beam splitters, for example, by means of additional crystal mirrors [50] or diamond diffraction gratings [46]. The gratings have an advantage over the crystal mirrors: they can be rather thick, whereas the crystals must be comparatively thin in a scale of tens of micrometers, which can result in stability problems. In case of the gratings, it is possible to use the first diffraction orders for outputting, or even to use a zero order for outputting in case of high amplification, while using diffraction orders as nucleation for subsequent circular bypasses of the cavity.

Conclusion

The X-ray resonators that were considered in the sections 1-3 of the review were once designed as an alternative to multi-crystal monochromators with the narrow spectrum transmittance bandwidth. However, a short insight into the history of creating and using the crystal cavity for Xray radiation leads to the conclusion that they were not/are not very popular for researchers as tools for investigating structural specific features of solid bodies and processes therein that are caused by external effects. Nevertheless, one should note their influence on creation of the crystal cavities for the X-ray free-electron lasers. First of all, the studies of Cotterill [3], Bond et al. [1] paved the way for designing a complanar and a noncomplanar cavity with variable pulse energy, respectively. Secondly, the X-ray cavity based on the two Bragg mirrors of backscattering is literally "copied" from the X-ray Fabry-Perot resonator. A crucial difference is just that the cavity size is determined by the distance between the electron FEL bunches in the first case and the wavelength of radiation in the second case.

Application of the crystal cavity in the X-ray free-electron lasers opens new opportunities for studying interrelation between the structure of matter and its dynamics. Moreover, X-ray methods which are presently limited by a spectrum flux, spatial and time coherency will greatly benefit from such a symbiosis. With picosecond and femtosecond pulses and their improved spectral characteristics, it will be possible to identify main mechanisms of non-equilibrium processes and structural phase transitions. good transverse coherency, extremely large longitudinal coherency and very short duration of the pulse, the Xray photon-correlated spectroscopy will take an advantage of increasing the coherent flux by three orders, thereby closing a time gap between the synchrotron radiation sources and the X-ray lasers. One may expect disclosure of completely new fields of research, for example, for methods of nuclear resonance scattering. It will make it possilbe to set the Mössbauer science beyond a mode of separate photons to open new perspectives for X-ray quantum optics, thereby allowing studying basics of collective and non-linear

interaction of light and matter [6]. In the future, it is possible to predict designing of a nuclear clock that is based, for example, on ⁴⁵Sc. Achievement of this goal will require further increase of the resonance spectral flux by means of improved the narrow-band sources of X-ray radiation [51].

Funding

This study was carried out under the state assignment of the National Research Center "Kurchatov Institute".

Conflict of interest

The author declares that he has no conflict of interest.

References

- [1] W.L. Bond, M.A. Duguay, P.M. Rentzepis. Appl. Phys. Lett., 10 (8), 216 (1967). DOI: 10.1063/1.1754919
- [2] R.D. Deslettes. Appl. Phys. Lett., 12 (4), 133 (1968).DOI: 10.1063/1.1651924
- [3] R.M.J. Cotterill. Appl. Phys. Lett., 12 (12), 403 (1968).DOI: 10.1063/1.1651874
- [4] R.T. Gabrielyan, A.H. Toneyan, O.S. Semerjyan. J. Contemp. Phys., 42 (2), 75 (2007). DOI: 10.3103/S1068337207020075
- R.R. Lindberg, K.-J. Kim, Yu. Shvyd'ko, W.M. Fawley. Phys. Rev. ST Accel. Beams, 14 (1), 010701 (2011).
 DOI: 10.1103/PhysRevSTAB.14.010701
- [6] B. Adams, G. Aeppli, T. Allison, A.Q.R. Baron, P. Bucksbaum, A.I. Chumakov, C. Corder, S.P. Cramer, S. DeBeer, Y. Ding, J. Evers, J. Frisch, M. Fuchs, G. Grübel, J.B. Hastings, Ch.M. Heyl, L. Holberg, Zh. Huang, T. Ishikawa, A. Kaldun, K.-J. Kim, T. Kolodziej, J. Krzywinski, Zh. Li, W.-T. Liao, R. Lindberg, A. Madsen, T. Maxwell, G. Monaco, K. Nelson, A. Palffy, G. Porat, W. Qin, T. Raubenheimer, D.A. Reis, R. Röhlsberger, R. Santra, R. Schoenlein, V. Schünemann, O. Shpyrko, Yu. Shvyd'ko, Sh. Shwartz, A. Singer, S.K. Sinha, M. Sutton, K. Tamasaku, H.-Ch. Wille, M. Yabashi, J. Ye, D. Zhu. arXiv: 1903.09317 (2019).
- [7] M.A. Mesropyan, A.G. Rostomyan. Izv. AN Armenii. Fizika, 26 (2), 71 (1991) (in Russian).
- [8] A.V. Kolpakov, R.N. Kuz'min, V.M. Ryaboy. J. Appl. Phys., 41 (8), 3549 (1970). DOI: 10.1063/1.1659460
- [9] N.N. Nasonov. Phys. Lett. A, 260 (5), 391 (1999).DOI: 10.1016/S0375-9601(99)00545-9
- [10] K. Kohra, T. Matsushita. Z. Naturforsch A, 27 (3), 484 (1972). DOI: 10.1515/zna-1972-0317
- [11] V.V. Lider. Crystallogr. Rep., 57 (5), 628 (2012).DOI: 10.1134/S1063774512050094
- [12] K.-D. Liss, R. Hock, M. Gomm, B. Waibel, A. Magerl, M. Krisch, R. Tucoulou. Nature, 404 (6776), 371 (2000). DOI: 10.1038/35006017
- [13] K.-D. Liss, R. Hock, M. Gomm, B. Waibel, A. Magerl, M. Krisch, R. Tucoulou. Proc. SPIE, 4143, 78 (2001). DOI: 10.1117/12.413682
- [14] C. Fabry, A. Pérot. Ann. Chim. Phys., 16 (7), 115 (1899).
- [15] A. Steyerl, K.-A. Steinhauser. Z. Physik B, 34 (2), 221 (1979). DOI: 10.1007/BF01322144

- [16] S.-L. Chang, Yu.P. Stetsko, M.-T. Tang, Y.-R. Lee, W.-H. Sun, M. Yabashi, T. Ishikawa, H.-H. Wu, B.-Y. Shew, Y.-H. Lin, T.-T. Kuo, K. Tamasaku, D. Miwa, S.-Y. Chen, Y.-Y. Chang, J.-T. Shy. Phys. Rev. B, 74 (13), 134111 (2006).
 DOI: 10.1103/PHYSREVB.74.134111
- [17] A. Caticha, S. Caticha-Ellis. Phys. Stat. Sol. (a), 119 (2), 643 (1990). DOI: 10.1002/pssa.2211190228
- [18] A. Caticha, K. Aliberty, S. Caticha-Ellis. Rev. Sci. Instrum., 67 (9), 3380 (1996). DOI: 10.1063/1.1147321
- [19] Y.V. Shvyd'ko, E. Gerdau. Hyp. Interact, **123/124** (1–4), 741 (1999). DOI: 10.1023/A:1017048629185
- [20] V.G. Kohn, Y.V. Shvyd'ko, E. Gerdau. Phys. Stat. Sol. (b), **221** (2), 597 (2000). DOI: 10.1002/1521-3951(200010)221:2₁597::AID-PSSB597;3.3.CO;2-N
- [21] Y.V. Shvyd'ko. X-ray resonators and other applications of Bragg backscattering. Habilitationsschrift (DESY, Hamburg, 2002), DOI: 10.3204/DESY-THESIS-2002-028
- [22] Y.V. Shvyd'ko. X-Ray Optics. Springer, Ser. Optical Science (Springer, Verlag, Berlin 2004), v. 98. DOI: 10.1007/978-3-540-40890-1
- [23] X.R. Huang, D.P. Siddons, A.T. Macrander, R.W. Peng,
 X.S. Wu. Phys. Rev. Lett., 108 (22), 224801 (2012).
 DOI: 10.1103/PhysRevLett.108.224801
- [24] Y.V. Shvyd'ko, M. Lerche, H.-C. Wille, E. Gerdau, M. Lucht, H.D. Rüter, E.E. Alp, R. Khachatryan. Phys. Rev. Lett., 90 (1), 013904 (2003). DOI: 10.1103/physr evlett.90.013904
- [25] S.-L. Chang, Yu.P. Stetsko, M.-T. Tang, Y.-R. Lee, W.-H. Sun,
 M. Yabashi, T. Ishikawa. Phys. Rev. Lett., 94 (17), 174801 (2005). DOI: 10.1103/PhysRevLett.94.174801
- [26] Y.W. Tsai, Y.H. Wu, Y.Y. Chang, W.C. Liu, H.L. Liu, C.H. Chu, P.C. Chen, P.T. Lin, C.C. Fu, S.L. Chang. J. Synchrotron Rad., 23 (3), 658 (2016). DOI: 10.1107/S1600577516004999
- [27] E. Burkel. Rep. Prog. Phys., 63 (2) P. 171 (2000).DOI: 10.1088/0034-4885/63/2/203
- [28] T. Toellner. Hyp. Int., **125** (1–4), 3 (2000). DOI: 10.1023/A:1012621317798
- [29] R. Fitzgerald. Phys. Today, 53 (7), 23 (2000).DOI: 10.1063/1.1292471
- [30] P. Emma, R. Akre, J. Arthur, R. Bionta, C. Bostedt, J. Bozek, A. Brachmann, P. Bucksbaum, R. Coffee, F.-J. Decker, Y. Ding, D. Dowell, S. Edstrom, A. Fisher, J. Frisch, S. Gilevich, J. Hastings, G. Hays, Ph. Hering, Z. Huang, R. Iverson, H. Loos, M. Messerschmidt, A. Miahnahri1, S. Moeller, H.-D. Nuhn, G. Pile, D. Ratner, J. Rzepiela, D. Schultz, T. Smith, P. Stefan, H. Tompkins, J. Turner, J. Welch, W. White, J. Wu, G. Yocky, J. Galayda. Nat. Photonics, 4 (9), 641 (2010).
 DOI: 10.1038/nphoton.2010.176
- [31] N. Huang, H. Deng, B. Liu, D. Wang, Z. Zhao. Innovation (Camb), 2 (2), 100097 (2021). DOI: 10.1016/j.xinn.2021.100097.
- [32] C. Feng, H.-X. Deng. Nucl. Sci. Tech., 29 (11), 160 (2018). DOI: 10.1007/s41365-018-0490-1
- [33] J. Feldhaus, E.L. Saldin, J.R. Schneider, E.A. Schneidmiller, M.V. Yurkov. Opt. Commun., 140 (4–6), 341 (1997). DOI: 10.1016/s0030-4018(97)00163-6

- [34] I. Nam, C.-K. Min, B. Oh, G. Kim, D. Na, Y.J. Suh, H. Yang, M.H. Cho, C. Kim, M.-J. Kim, Ch.H. Shim, J.H. Ko, H. Heo, J. Park, J. Kim, S. Park, G. Park, S. Kim, S.H. Chun, H. Hyun, J.H. Lee, K.S. Kim, I. Eom, S. Rah, D. Shu, K.-J. Kim, S. Terentyev, V. Blank, Yu. Shvyd'ko, S.J. Lee, H.-S. Kang. Nat. Photonics, 15 (6), 435 (2021).
 DOI: 10.1038/s41566-021-00777-z
- [35] K.-J. Kim, Y. Shvyd'ko, S. Reiche. Phys. Rev. Lett., 100 (24), 244802 (2008). DOI: 10.1103/physrevlett.100.244802
- [36] K.-J. Kim, Y.V. Shvyd'ko. Phys. Rev. ST Accel. Beams, 12 (3), 030703 (2009). DOI: 10.1103/PhysRevSTAB.12.030703
- [37] Z. Huang, R. D. Ruth. Phys. Rev. Lett., **96** (14), 144801 (2006). DOI: 10.1103/physrevlett.96.144801
- [38] H.P. Freund, P.J.M. van der Slot, Yu. Shvyd'ko. New J. Phys.,21 (9), 093028 (2019). DOI: 10.1088/1367-2630/ab3f72
- [39] G. Marcus, A. Halavanau, Z. Huang, J. Krzywinski, J. MacArthur, R. Margraf, T. Raubenheimer, D. Zhu. Phys. Rev. Lett., 125 (25), 254801 (2020). DOI: 10.1103/PhysRevLett.125.254801
- [40] T. Liu, Z. Qi, W. Zhang, S.-W. Xiang, Y.-Y. Lei, Y. Zhu, Y.-Z. He, Q.-B. Yuan, F. Gao, R.-B. Deng, S. Sun, Z.-D. Lei, Z.-Q. Jiang, M.-Q. Duan, Y. Zhuan, X.-F. Huang, Y.-Y. Lei, Y. Zhu, Y.-Zh. He, Q.-B. Yuan, F. Gao, R.-B. Deng, S. Sun, Zh.-D. Lei, Zh.-Q. Jiang, M.-Q. Duan, Yu. Zhuan, X.-F. Huang, P.-Ch. Dong, Zh.-L. Li, Sh.-Y. Si, L. Xue, S. Chen, Y.-F. Liu, Y.-J. Tong, H.-X. Deng, Zh.-T. Zhao. Nucl. Sci. Tech., 34, 6 (2023). DOI: 10.1007/s41365-022-01151-6
- [41] P. Liu, P. Pradhan, A. Miceli, D.A. Walko, D. Shu, J. Sullivan, K. Lang, M. Rivers, M. Balcazar, K. Li, R. Margraf, A. Halavanau, A. Sakdinawat, T. Sato, D. Zhu, Y. Shvyd'ko. Phys. Rev. Accel. Beams, 27 (11), 110701 (2024). DOI: 10.1103/Phys-RevAccelBeams.27.110701
- [42] P. Rauer, W. Decking, D. Lipka, D. Thoden, T. Wohlenberg. Phys. Rev. Accel. Beams, 26 (2), 020701 (2023). DOI: 10.1103/PhysRevAccelBeams.26.020701
- [43] A. Snigirev, V. Kohn, I. Snigireva, B. Lengeler. Nature, 384 (6604), 49 (1996). DOI: 10.1038/384049a0
- [44] Y.V. Shvyd'ko, V. Blank, S. Terentyev. MRS Bull., 42 (06), 437 (2017). DOI: 10.1557/mrs.2017.119
- [45] P.J.M. van der Slot, H.P. Freund. Appl. Sci., **11** (11), 4978 (2021). DOI: 10.3390/app11114978
- [46] R. Margraf, R. Robles, A. Halavanau, J. Kryzywinski, K. Li, J. MacArthur, T. Osaka, A. Sakdinawat, T. Sato, Y. Sun, K. Tamasaku, Z. Huang, G. Marcus, D. Zhu. Nat. Photonics, 17 (10), 878 (2023). DOI: 10.1038/s41566-023-01267-0
- [47] M. Singleton, J. Rosenzweig, J. Tang, Z. Huang. Instruments, 8 (1), 2 (2024). DOI: 10.3390/instruments8010002
- [48] J.B. Rosenzweig, N. Majernik, R.R. Robles, G. Andonian, O. Camacho, A. Fukasawa, A. Kogar, G. Lawler, J. Miao, P. Musumeci, B. Naranjo, Y. Sakai, R. Candler, B. Pound, C. Pellegrini, C. Emma, A. Halavanau, J. Hastings, Z. Li, M. Nasr, S. Tantawi, P. Anisimov, B. Carlsten, F. Krawczyk, E. Simakov, L. Faillace, M. Ferrario, B. Spataro, S. Karkare, J. Maxson, Y. Ma, J. Wurtele, A. Murokh, A. Zholents, A. Cianchi, D. Cocco, S.B. van der Geer. New J. Phys., 22 (9), 093067 (2020). DOI: 10.1088/1367-2630/abb16c
- [49] T. Kolodziej, P. Vodnala, S. Terentyev, V. Blank, Y.J. Shvyd'ko. Appl. Cryst., 49 (4), 1240 (2016). DOI: 10.1107/S1600576716009171
- [50] Y.V. Shvyd'ko. Phys. Rev. Accel. Beams, 22 (10), 100703 (2019). DOI: 10.1103/physrevaccelbeams.22.100703

[51] Y. Shvyd'ko, R. Röhlsberger, O. Kocharovskaya, J. Evers, G.A. Geloni, P. Liu, D. Shu, A. Miceli, B. Stone, W. Hippler, B. Marx-Glowna, I. Uschmann, R. Loetzsch, O. Leupold, H.-C. Wille, I. Sergeev, M. Gerharz, X. Zhang, Ch. Grech, M. Guetg, V. Kocharyan, N. Kujala, Sh. Liu, W. Qin, A. Zozulya, J. Hallmann, U. Boesenberg, W. Jo, J. Möller, A. Rodriguez-Fernandez, M. Youssef, A. Madsen, T. Kolodziej. Nature, 622 (7983), 1 (2023).
DOI: 10.1038/s41586-023-06491-w

Translated by M.Shevelev